AAC Journals.ASM.org

A Novel Antimycobacterial Compound Acts as an Intracellular Iron Chelator

Marte S. Dragset,[a,b,c] Giovanna Poce,[a,d] Salvatore Alfonso,[a,d] Teresita Padilla-Benavides,[f] Thomas R. Ioerger,[g] Takushi Kaneko,[h] James C. Sacchettini,[i] Mariangela Biava,[d] Tanya Parish,[j] José M. Argüello,[f] Magnus Steigedal,[a,c,e] Eric J. Rubin[a]

Department of Immunology and Infectious Diseases, Harvard School of Public Health, Boston, Massachusetts, USA[a]; Department of Biotechnology, Norwegian University of Science and Technology, Trondheim, Norway[b]; Centre of Molecular Inflammation Research and Department of Cancer Research and Molecular Medicine, Norwegian University of Science and Technology, Trondheim, Norway[c]; Dipartimento di Chimica e Tecnologie del Farmaco, Sapienza University of Rome, Rome, Italy[d]; Central Norway Regional Health Authority, Stjørdal, Norway[e]; Department of Chemistry and Biochemistry, Worcester Polytechnic Institute, Worcester, Massachusetts, USA[f]; Department of Computer Science and Engineering, Texas A&M University, College Station, Texas, USA[g]; Global Alliance for TB Drug Development, New York, New York, USA[h]; Department of Biochemistry and Biophysics, Texas A&M University, College Station, Texas, USA[i]; Infectious Disease Research Institute, Seattle, Washington, USA[j]

Efficient iron acquisition is crucial for the pathogenesis of *Mycobacterium tuberculosis*. Mycobacterial iron uptake and metabolism are therefore attractive targets for antitubercular drug development. Resistance mutations against a novel pyrazolopyrimidinone compound (PZP) that is active against *M. tuberculosis* have been identified within the gene cluster encoding the ESX-3 type VII secretion system. ESX-3 is required for mycobacterial iron acquisition through the mycobactin siderophore pathway, which could indicate that PZP restricts mycobacterial growth by targeting ESX-3 and thus iron uptake. Surprisingly, we show that ESX-3 is not the cellular target of the compound. We demonstrate that PZP indeed targets iron metabolism; however, we found that instead of inhibiting uptake of iron, PZP acts as an iron chelator, and we present evidence that the compound restricts mycobacterial growth by chelating intrabacterial iron. Thus, we have unraveled the unexpected mechanism of a novel antimycobacterial compound.

Iron is an essential nutrient for almost all living organisms. While ferric iron (Fe^{3+}) is nearly insoluble in aqueous solutions under aerobic conditions and neutral pH, the soluble ferrous iron (Fe^{2+}) is potentially toxic to the cell due to generation of deleterious oxygen radicals through participation in Fenton chemistry (1). Thus, the amount of soluble iron is tightly regulated within organisms (1). *Mycobacterium tuberculosis*, the causative agent of tuberculosis (TB), infects macrophages and resides within the low-iron environment of the phagosome (2, 3). To overcome iron starvation, *M. tuberculosis* produce high-affinity Fe^{3+}-chelating siderophores called mycobactin/carboxymycobactin (the latter a soluble variant of mycobactin; here we refer to both as mycobactins) to enhance iron uptake from the surroundings (4, 5). Nonpathogenic mycobacteria, like *Mycobacterium smegmatis*, produce a second structurally different siderophore, exochelin, in addition to the mycobactins (6, 7). When entering bacterial cells by means of siderophores, Fe^{3+} is reduced to Fe^{2+} for incorporation into mycobacterial iron-containing proteins, including iron storage proteins like bacterioferritin (1). Other known mycobacterial iron uptake mechanisms include heme uptake (8, 9), internalization of holo-transferrin (10), and low-affinity iron uptake through outer membrane porins (11). Guinea pigs and mice infected by *M. tuberculosis* strains deficient in siderophore synthesis or transport across the cell membrane show a significant reduction in bacterial burden compared to animals infected by wild-type (WT) *M. tuberculosis* (12, 13), demonstrating the need for iron in mycobacterial virulence.

TB is responsible for 1.5 million deaths per year, and the growing resistance toward current TB drugs calls for urgent identification of new mycobacterial drug targets (14–16). As part of a high-throughput drug target identification screen, we previously identified mutations within the *eccB3* gene of the mycobacterial *esx-3* gene cluster which conferred resistance to the novel antitubercular pyrazolopyrimidinone compound PZP {3-(4-chlorophenyl)-5-(cyclohexylmethyl)pyrazolo[1,5-α]pyrimidin-7(4*H*)-one}(15) (Fig. 1A). For potential lead optimization, it is beneficial to unravel both the target and mechanism of action of a new compound at an early stage of development. In this study, we sought to identify the target and mechanism of PZP.

The *esx-3* gene cluster comprises a set of 11 genes, as indicated in Fig. 1B, that encode the ESX-3 type VII secretion system (17). The specific role of *eccB3* in ESX-3 function is currently unknown. Interestingly, ESX-3 is known to be required for the mycobactin-mediated siderophore iron uptake pathway (18–21). ESX-3 is essential in *M. tuberculosis* but not in *M. smegmatis*, which, in addition to mycobactins, produces exochelin that functions independently of ESX-3. However, ESX-3 is still absolutely required for mycobactin-mediated iron uptake in the latter species (18, 20). This nonessential nature of ESX-3 in *M. smegmatis* has previously proven to be of great advantage when resolving mechanisms re-

Received 29 December 2014 **Returned for modification** 17 January 2015
Accepted 22 January 2015

Accepted manuscript posted online 2 February 2015

Citation Dragset MS, Poce G, Alfonso S, Padilla-Benavides T, Ioerger TR, Kaneko T, Sacchettini JC, Biava M, Parish T, Argüello JM, Steigedal M, Rubin EJ. 2015. A novel antimycobacterial compound acts as an intracellular iron chelator. Antimicrob Agents Chemother 59:2256–2264. doi:10.1128/AAC.05114-14.

Address correspondence to Eric J. Rubin, erubin@hsph.harvard.edu, or Magnus Steigedal, magnus.steigedal@ntnu.no.

M.S. and E.J.R. contributed equally to this work.

Supplemental material for this article may be found at http://dx.doi.org/10.1128/AAC.05114-14.

doi:10.1128/AAC.05114-14

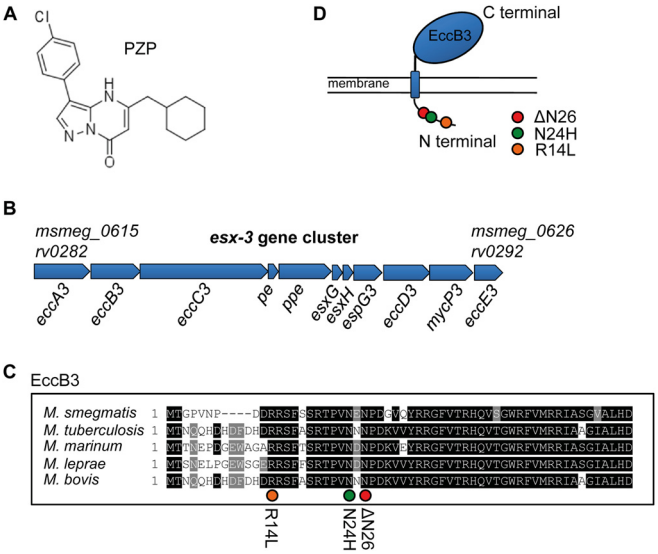

FIG 1 Clones of *M. tuberculosis* resistant to PZP have mutations in the *eccB3* gene of ESX-3. (A) Chemical structure of PZP. (B) The *esx-3* gene cluster is composed of 11 genes stretching from MSMEG_0615 to MSMEG_0626 in *M. smegmatis* (SmegmaList, http://mycobrowser.epfl.ch/smegmalist.html) and *rv0282* to *rv0292* in *M. tuberculosis* (TubercuList, http://tuberculist.epfl.ch/index.html). (C) Amino acid sequence of the N-terminal end of EccB3. Black highlighting indicates conserved residues in mycobacteria. Orange, green, and red circles indicate the locations of mutated residues in PZP-resistant *M. tuberculosis* (R14L, N24H, and ΔN26 mutations). (D) EccB3 is a transmembrane protein with a predicted small (the first 71 amino acids) cytosolic tail on the N terminus and a large (amino acid 95 to 538) extracellular C-terminal domain. The mutations R14L, N24H, and ΔN26 are localized to the cytosolic tail, as indicated.

lated to ESX-3 and mycobactin iron metabolism (18). Therefore, we aimed to unravel the target and mechanism of PZP in *M. smegmatis*. We initially hypothesized that treatment with PZP would block ESX-3 function and decrease mycobacterial iron uptake. Paradoxically, treatment with the compound increased bacterial iron levels, but treated cells behaved as if they were starved for iron. We found that, instead of acting directly on ESX-3, PZP is a chelator of Fe^{2+} that apparently deprives the microbe of access to its own intracellular pools of iron.

MATERIALS AND METHODS

Strains and culture conditions. The parental bacterial strain used in this study was *Mycobacterium smegmatis* mc^2155 (22), and mutant strains used in this study are listed in Table 1. To monitor growth of *M. smegmatis* strains in iron-deplete or -replete medium, the bacteria were first grown to stationary phase in Middlebrook 7H9 (BD Difco) supplemented with 0.2% glycerol, 0.05% Tween 80, and 10% albumin-dextrose-catalase (ADC) medium (5% [wt/vol] bovine serum albumin fraction V, 2% [wt/vol] dextrose, 145.5 mM NaCl, 0.003% [wt/vol] catalase). The cells were then centrifuged at 3,000 × *g* for 10 min and washed once in chelated Sauton's medium prepared as previously described, using Chelex100 (Bio-Rad) (18). When growth of the WT and *eccB3*(ΔN26) mutant strains was compared (see Fig. 3C and D, below), cultures were not washed, in order to slightly relax the low-iron growth conditions. The cultures were diluted to an optical density at 600 nm (OD_{600}) of 0.01 in chelated Sauton's medium with 100 μM 2,2′-bipyridine (Alfa Aesar) for iron-deplete (low-iron) conditions or with 150 μM $FeCl_3$ for iron-replete (high-iron) conditions. Growth was monitored in microplate honeycomb wells (Oy Growth Curves Ab Ltd.), with 200 μl in each well, using a Bioscreen growth curve reader (Oy Growth Curves Ab Ltd.). The growth was also assessed by growing 10 ml of culture in 50-ml plastic tubes and measuring the OD_{600}, using a standard spectrophotometer.

Construction of *M. smegmatis* mutant strains. An *M. smegmatis* mutant unable to synthesize exochelin (Δ*fxbA*) was created by replacing the formyl transferase *fxbA* (MSMEG_0014 [SmegmaList, http://mycobrowser.epfl.ch/smegmalist.html]), with the hygromycin resistance (HygR) gene by recombineering (23). A fragment containing the 200 bp flanking *fxbA* separated by the linker AGATCTGTCCTACTCGAG, where the underlined sequences are the restriction sites for BglII and XhoI, was synthesized and cloned into pUC57-simple (Genscript, USA) (see Fig. S1 in the supplemental material). The HygR cassette was amplified from pUV15TetORm (24) by using primers BamHIHygF (AGATGGATCCTGACGTTCATCCATAGTTGCCTG) and XhoIHygR (AGATCTCGAGGCGGCTTTAGCTAATTAATTGG) and cloned into the BglII and XhoI sites of the flanking sequences. The flanked HygR cassette was amplified using primers KO_FxbA_F (TTCGCGATGCTCAACCGCGA) and KO_FxbA_R (CGTCGTTGACCAGGACCACG). Allelic exchange with *fxbA* and the HygR cassette was carried out by transforming the amplified product into an *M. smegmatis* strain expressing the mycobacteriophage recombinases gp60 and gp61 on a nitrile-inducible, counterselectable episomal plasmid. The recombineering plasmid was removed by counterselecting on 10% sucrose. Successful replacement of *fxbA* with the HygR cassette was confirmed by Southern blot analysis (data not shown).

The *M. smegmatis* point mutants *eccB3*(R14L), *eccB3*(N24H), and *eccB3*(ΔN26) were constructed by single-stranded DNA recombineering (25) using the tetracycline-inducible, gp61-expressing vector pKM402 (kind gift from Kenan Murphy, University of Massachusetts Medical School, MA, USA). Tetracycline-induced *M. smegmatis* containing pKM402 was cotransformed with 1 μg of the oligonucleotide RpsL (CGCGCGCGACCTTCCGGAGGGCCGAGTTCGGCTTCCTCGGAGTGGTGGTGTAAACGCGCGTGCACACGCC), which introduced a point mutation in the *M. smegmatis rpsL* locus, which confers resistance to streptomycin, and the oligonucleotide R14L (CTCGTTGACCGGGGTGCGCGAGCTGAACGAGCGCAGGTCGTCGGGGTTGACGGGGCCGGTATGCCGGCA), N24H (CCGCGGCGGTACTGCACGCCGTCGGGGTTCTCGTGGACCGGGGTGCGCGAGCTGAACGAGCGCCGGTCGT), or ΔN26 (GTGACGAAACCGCGGCGGTACTGCACGCCGTCGGGCTCGTTGACCGGGGTGCGCGAGCTGAACGAGCGC), which introduced the specific point mutations in *eccB3*. RpsL mutants were selected on LB plates containing 20 μg/ml streptomycin, and a mismatch amplification mutation assay (MAMA)-PCR was used to identify the second desired mutation in the *eccB3* gene (26). Positive mutants were confirmed by sequencing.

Chemical materials. PZP was synthesized at BioDuro Beijing Co., Ltd. Ferrozine {3-(2-pyridyl)-5,6-diphenyl-1,2,4-triazine-*p*,*p*′-disulfonic acid monosodium salt hydrate}, ferrous sulfate heptahydrate, and hydroxylamine hydrochloride were purchased from Sigma-Aldrich. PZP was dissolved in dimethyl sulfoxide (DMSO), ferrozine was dissolved in deionized water, and ferrous sulfate heptahydrate was freshly prepared in 0.1 M HCl. Hydroxylamine hydrochloride was dissolved in 2 N HCl (final concentration, 1.4 M). The solutions were kept at 4°C until use.

TABLE 1 Strains used in this study

M. smegmatis strain	Reference	Siderophore(s) produced[a]	Functional siderophore[a] iron uptake pathway(s)
mc^2155	22	M, E	M, E
Δ*esx-3*	18	M, E	E
Δ*esx-3 fxbA::pSES*	18	M	None
Δ*fxbA*	This study	M	M
eccB3(R14L)	This study	M, E	M*, E
eccB3(N24H)	This study	M, E	M*, E
eccB3(ΔN26)	This study	M, E	M*, E

[a] M, mycobactin/carboxymycobactin; E, exochelin; *, unverified.

***M. smegmatis* sensitivity assay.** Determination of the *M. smegmatis* PZP MIC under iron-replete conditions was based on a resazurin microtiter assay (27). Briefly, *M. smegmatis* was grown to stationary phase before dilution to an OD_{600} of 0.001, added in triplicate to 96-well plates, and grown with shaking at 37°C in the presence of increasing concentrations of PZP for 24 h before addition of 0.02% of resazurin (Sigma). The cultures were incubated for another 16 h before the color of the cultures was analyzed. Pink and blue distinguishes metabolically active and inactive *M. smegmatis* cultures, respectively. The PZP MIC under iron-deplete conditions was determined by monitoring growth in increasing concentrations of compound in a Bioscreen growth curve reader; the MIC was defined as the lowest concentration of PZP that prevented growth after 60 h growth with shaking at 37°C.

Iron content analysis. Whole-cell metal content was measured in *M. smegmatis* WT and *eccB3*(ΔN26) mutant strains grown to the late exponential phase in low- or high-iron Sauton's medium and in the presence or absence of 25 μM PZP for 24 h. Cells were washed three times in 5 ml of buffer containing 50 mM HEPES (pH 7.5) and 500 mM NaCl (all glassware was previously rinsed with deionized H_2O plus 5% HNO_3, trace metal grade). The samples were resuspended in 100 μl deionized H_2O, and a 10-μl aliquot was used for protein content determination (28). The remaining 90 μl of each sample was acid digested with 200 μl HNO_3 (trace metal grade) for 1 h at 80°C and overnight at 20°C. Digestions were concluded after addition of 60 μl of 30% H_2O_2 and dilution to 2 ml with water. Metal content in digested samples was measured by atomic absorption spectroscopy (Analyst 300; PerkinElmer, Foster City, CA, USA).

RNA extraction and quantitative RT-PCR. Total RNA extraction, cDNA synthesis, quantitative reverse transcription-PCR (RT-PCR), and analysis were performed as previously described by Siegrist et al. (18), using primers targeting *M. smegmatis mbtB*, *mbtL*, *irtA*, and *sigA* (18).

ESI-MS studies. Electrospray ionization-mass spectrometry (ESI-MS) studies were carried out in an ESI-MS spectra recorder with an MSD SL Trap mass spectrometer (Agilent Technologies) equipped with an electrospray ionization source. Solutions were analyzed by direct injection. PZP was dissolved in water-methanol (1:1, vol/vol) to a final concentration of 10 μM, and a ferrous sulfate heptahydrate water solution was added at a molar ratio 1:1. Data were analyzed with the Thermo Scientific Xcalibur software.

UV-Vis titration of PZP with Fe^{2+}. UV-Vis (UV-visible) spectroscopic studies were performed in a PerkinElmer Lambda 10 spectrometer at room temperature (25°C). Standard 1-cm quartz cuvettes were used to hold sample and reference solutions. PZP was titrated by sequential addition of increasing amounts of Fe^{2+} solution to the same cuvette. Briefly, to a starting 10 μM PZP solution in DMSO-potassium phosphate buffer (20 mM, pH 7.2), increments of 1 μM ferrous sulfate water solution (freshly made in HCl and hydroxylamine; 1 mM stock solution) were added until a total concentration of 10 μM Fe^{2+} was reached, and then in 2 μM increments until a total concentration of 20 μM Fe^{2+} was reached. All titrations were performed in 20 mM potassium phosphate buffer, pH 7.2. All solutions were scanned from 240 to 800 nm.

Measurements of the binding constant. UV-Vis spectroscopic methods were used for determining apparent binding constants for the formation of PZP-Fe^{2+} complex in 20 mM potassium phosphate buffer, pH 7.2. First, the molar stoichiometry of the complexes formed by titration of 10 μM PZP with increasing amounts of Fe^{2+} was determined by monitoring the change of absorbance at 400 nm (the wavelength where the complexes absorb while the ligand does not). The method used was previously described for the determination of the apparent binding constant of the quercetin-Fe^{2+} complex (29). The spectroscopic measurements registered at 400 nm were used for the calculations.

Competition for Fe^{2+} between PZP and ferrozine. A solution of 3:1 ferrozine-Fe^{2+} (60 μM:20 μM) mixture in 1 ml of 20 mM potassium phosphate buffer (pH 7.2) was prepared in a 1-cm-path-length quartz cuvette. Sixty microliters of PZP (60 μM) was added to this solution after 30 min. The absorbance of the complex was measured every 30 min for 1.5 h.

RESULTS

***M. smegmatis* is not susceptible to PZP under iron-replete conditions.** Based on whole-genome sequencing of three *M. tuberculosis* mutants conferring resistance to PZP, we previously identified single mutations, all mapping to *rv0283* (*eccB3*), a gene encoding a putative transmembrane protein of unknown function within the *esx-3* gene cluster (15). Two of the clones encoded nonsynonymous EccB3 substitutions, R14L and N24H, while the third contained a frame-preserving 3-bp deletion that eliminated N26 from the primary EccB3 sequence (15). These residues are conserved among mycobacteria (Fig. 1C), and all three localize to the N-terminal cytosolic tail of EccB3, as predicted by the TMHMM software (30, 31) (Fig. 1D). *M. tuberculosis* is dependent on a functional ESX-3 system for growth (18, 20, 32–34), and all *M. tuberculosis* mutations conferring resistance to PZP were mapped to the *esx-3* gene cluster (15). These findings prompted us to investigate whether PZP could interfere with the activity of ESX-3 or, alternatively, if ESX-3 could be involved in PZP uptake. ESX-3 is essential in *M. tuberculosis*, but not in *M. smegmatis* (18, 20). Thus, if EccB3 is the cellular target of PZP, *M. smegmatis* should not be susceptible to the compound. Indeed, a resazurin microtiter assay showed that growth was not affected by PZP when included in the medium up to a 1 mM concentration (results not shown), and we concluded that *M. smegmatis* is not affected by PZP under these conditions.

***M. smegmatis* is susceptible to PZP under iron-depleted conditions.** An *M. smegmatis* strain disrupted in a gene encoding a formyl transferase (*fxbA*) required for exochelin biosynthesis shows slight growth restriction compared to the WT under iron-limited conditions (18). When the *esx-3* cluster, which is required for mycobactin-mediated iron uptake, is deleted in addition to the disrupted *fxbA* gene (Δ*esx-3 fxbA::pSES* mutant), *M. smegmatis* does not grow in low iron, since both the mycobactin and exochelin pathways are nonfunctional in this strain. However, an *esx-3* knockout with an additional mutation that abolishes mycobactin synthesis is disrupted in the mycobactin pathway only and thus grows under low-iron conditions due to production of exochelin (18). These findings showed that ESX-3 is required for iron acquisition through the mycobactin pathway but not the exochelin pathway (18). If PZP targets mycobactin-mediated iron uptake via ESX-3/EccB3, we reasoned that an *M. smegmatis* mutant unable to produce exochelin (Δ*fxbA*) would behave similarly to the Δ*esx-3 fxbA::pSES* double mutant and not grow in the presence of PZP under low-iron conditions. To test this hypothesis, we grew the Δ*fxbA* mutant in iron-deplete medium (100 μM 2,2′-bipyridine) in the presence of PZP. Surprisingly, PZP inhibited the growth of all strains under these conditions, including the WT, which we hypothesized would grow due to the production of exochelin (Fig. 2A, left). All strains were rescued by iron repletion (150 μM $FeCl_3$) (Fig. 2A, right). Thus, the action of PZP in *M. smegmatis* is dependent on low environmental iron.

PZP does not target the ESX-3 secretion system. Our results showed that production of exochelin could not rescue the cells from PZP, suggesting a mechanism of action independent of ESX-3. To further investigate whether the compound impairs mycobacterial growth independently of ESX-3, we analyzed the response of an Δ*esx-3* whole-locus deletion mutant to PZP. The

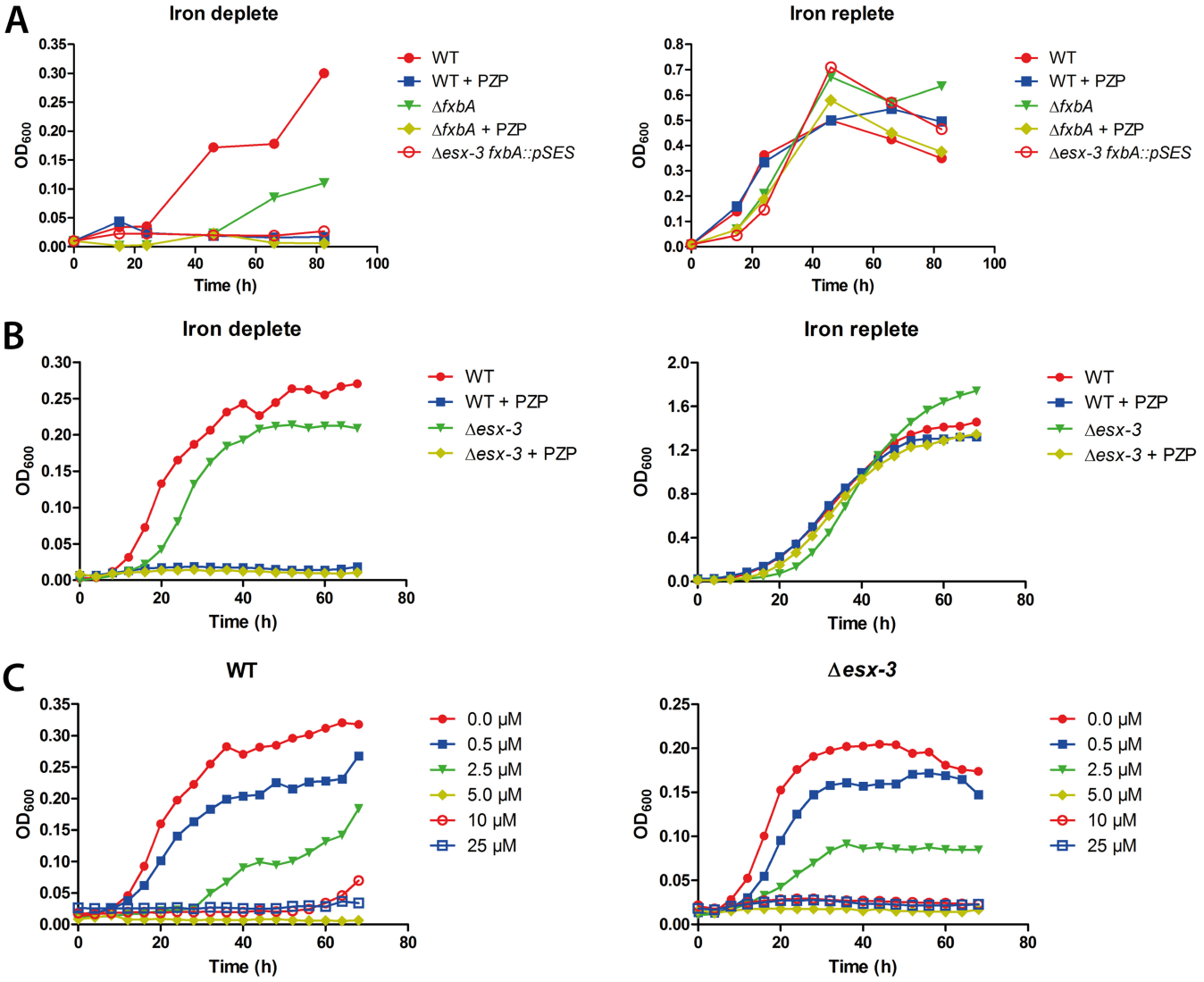

FIG 2 *M. smegmatis* is susceptible to PZP in an iron-dependent, ESX-3-independent manner. (A) Growth of *M. smegmatis* WT and Δ*fxbA* was monitored by OD_{600} measurements for 80 h under iron-replete (right) and iron-deplete (left) conditions, in the presence or absence of 25 μM PZP. *M. smegmatis* Δ*esx-3* Δ*fxbA* was included as a control. Results are representative of two independent experiments. (B) Growth of *M. smegmatis* WT and Δ*esx-3* was monitored for 70 h in iron-replete (right) and iron-deplete (left) medium, in the presence or absence of 25 μM PZP. (C) Growth of *M. smegmatis* WT (left) and Δ*esx-3* (right) was monitored for 70 h in iron-deplete medium in the presence of increasing concentrations of PZP. Results shown in panels B and C represent the averages of three independent biological replicates.

growth of the Δ*esx-3* mutant was slightly impaired at low iron levels but not at iron-replete levels compared to the WT strain (Fig. 2B). However, the growth of both Δ*esx-3* and WT strains was completely inhibited in the presence of PZP and rescued by the presence of iron (Fig. 2B). Furthermore, in low iron, the MICs for both WT and the Δ*esx-3* mutant were between 2.5 and 5 μM (Fig. 2C). Since the Δ*esx-3* mutant and WT strains showed similar sensitivities to PZP, we concluded that the compound does not target EccB3 or any other component of the ESX-3 system. In addition, ESX-3 does not appear responsible for uptake of the compound.

PZP leads to iron accumulation in *M. smegmatis*. Our observations suggested that PZP interferes with iron homeostasis. We hypothesized that the compound might interfere with iron uptake and expected that PZP treatment would result in decreased iron accumulation. To test this, we analyzed the whole-cell iron content by atomic absorption spectroscopy. *M. smegmatis* WT cells were grown in iron-replete or -deplete medium in the presence or absence of PZP. We found elevated iron levels in cells grown in replete medium compared to those grown under iron-deplete conditions (Fig. 3A, blue bars, minus PZP). Surprisingly, however, iron accumulation increased in the presence of PZP under iron-rich conditions (Fig. 3A, blue bars, replete). No difference in iron content was observed in cells grown in low-iron medium in the presence or absence of the compound (Fig. 3A, blue bars, deplete). Since iron accumulated in *M. smegmatis* WT under iron-rich conditions, we compared the iron content in mycobacteria containing the *eccB3 M. tuberculosis* resistance mutations. The R14, N24, and N26 residues are conserved among mycobacteria (Fig. 1C), suggesting that a mutation in these residues in *M. smegmatis* would have the same effect as the *M. tuberculosis* mutations.

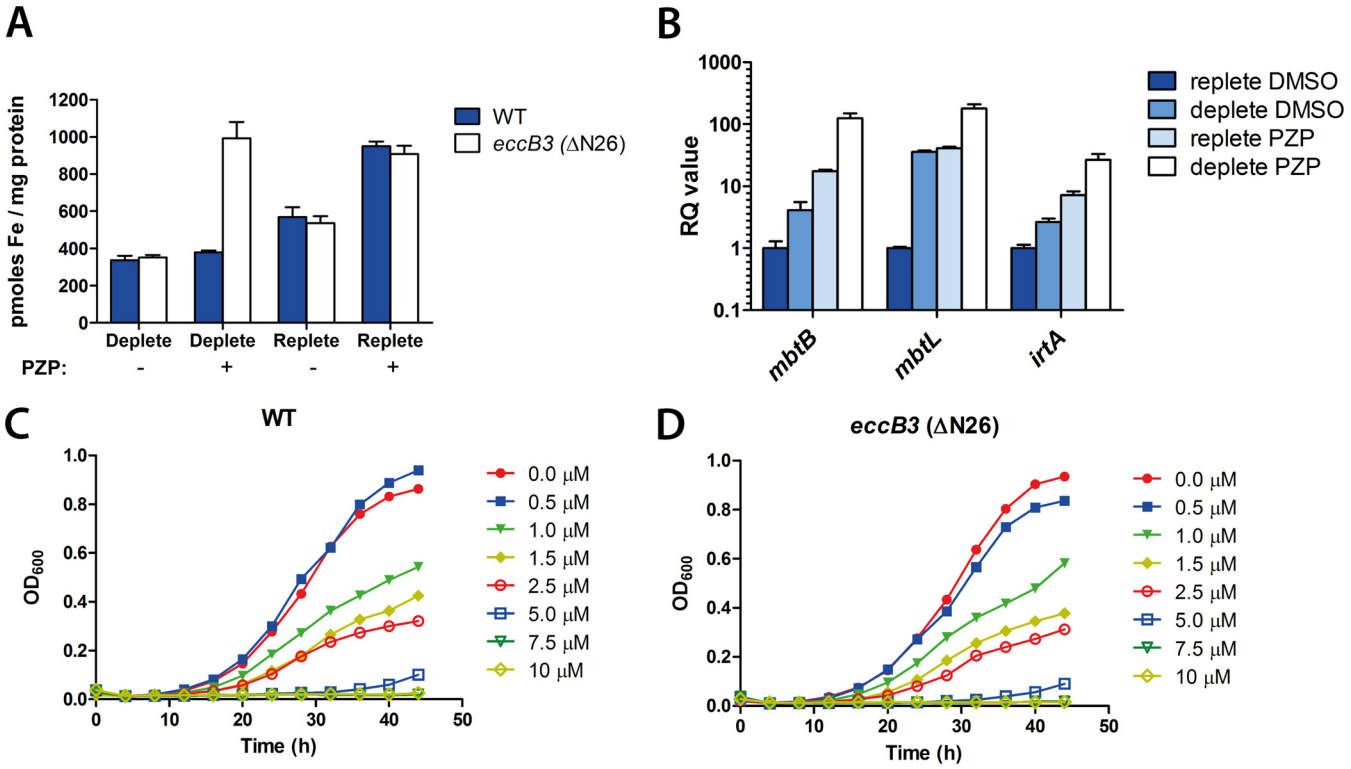

FIG 3 Treatment with PZP leads to iron accumulation and upregulation of iron uptake genes in *M. smegmatis*. (A) Whole-cell iron content was measured by atomic absorption spectroscopy in *M. smegmatis* WT and *eccB3*(ΔN26) strains grown to the late exponential phase in iron-deplete or iron-replete medium for 24 h in the presence (+) or absence (−) of 25 μM PZP. Error bars represent standard errors of at least five biological replicates. (B) *M. smegmatis* WT was grown in iron-deplete or iron-replete medium for 24 h in the presence (+) or absence (−) of 25 μM PZP. The relative transcript levels of three iron-responsive genes (*mbtB*, *mbtL*, and *irtA*) were measured by quantitative RT-PCR. Error bars represent the calculated maximum (RQ_{max}) and minimum (RQ_{min}) as determined from the standard errors of the cycle threshold changes (ΔC_T values). (C and D) *M. smegmatis* WT and *eccB3*(ΔN26) mutant strains were grown under iron-depleted conditions with increasing concentrations of PZP, and the OD_{600} was monitored every second hour.

Hence, we constructed an *M. smegmatis eccB3*(ΔN26) mutant strain and analyzed the iron levels. Increased iron accumulation was observed in the *eccB3*(ΔN26) mutant in the presence of the compound under both iron-replete and -deplete conditions (Fig. 3A, white bars). We speculate that the mutations in *eccB3* increase the iron acquisition-related activity of ESX-3, leading to increased iron influx. However, this mutant strain did not show increased resistance to PZP (Fig. 3C and D). Similarly, increased resistance to the compound was not observed in *M. smegmatis eccB3*(R14L) or *eccB3*(N24H) strains (results not shown). Given the rather small shift in the MICs for these mutations that have been reported elsewhere for *M. tuberculosis* (only a 2.5-fold shift under iron-rich conditions) (15), it is likely that there is substantial interplay between the environmental iron concentration and resistance, and it remains possible that one could detect resistance of *M. smegmatis eccB3* mutants under optimal iron conditions. Attempts to recreate PZP-resistant *eccB3* mutants in *M. tuberculosis* were not successful, perhaps due to the selection of resistant recombinants under suboptimal iron conditions (15). Nevertheless, these results certainly demonstrated that iron accumulates in mycobacterial cells in the presence of PZP when sufficient iron is available in the medium.

PZP-treated *M. smegmatis* upregulates iron acquisition genes. Mycobacteria sense iron availability and upregulate acquisition systems in response to iron starvation (35). The increased iron accumulation seen in the presence of PZP suggested that cells sense iron starvation and should, therefore, show upregulated iron acquisition gene expression. Several genes are known to be iron regulated, including *mbtB* and *mbtL*, both of which are involved in mycobactin synthesis but are located in separate gene clusters (36). Another iron-responsive gene, *irtA*, encodes a mycobactin transporter suggested to couple siderophore import and iron assimilation together with IrtB (12, 37). Thus, we measured the expression levels of *mbtB*, *mbtL*, and *irtA* in *M. smegmatis* cells in the presence and absence of PZP. Under iron-deplete conditions, higher expression of iron uptake genes was observed than under iron-replete conditions (Fig. 3B). All three iron-responsive genes were, however, further upregulated in the presence of the compound under both high- and low-iron conditions (Fig. 3B). Thus, although cells accumulate increased amounts of iron in the presence of PZP, they simultaneously sense iron starvation.

PZP chelates Fe^{2+}. We found that cells treated with PZP accumulate iron but at the same time sense iron starvation. Aiming to resolve these seemingly contradictory observations, we noted that PZP has a pyrazolo-[1,5α]pyrimidinone core that potentially possesses Fe^{2+}-chelating properties. Thus, we investigated whether the compound could complex with iron by using ESI-MS with direct injection of solutions of PZP and Fe^{2+}. Figure 4 shows the ESI-MS spectra of PZP (Fig. 4A) and PZP plus 1 mole equivalent of Fe^{2+} (Fig. 4B). In addition to the free ligand PZP (*m/z* 364.17,

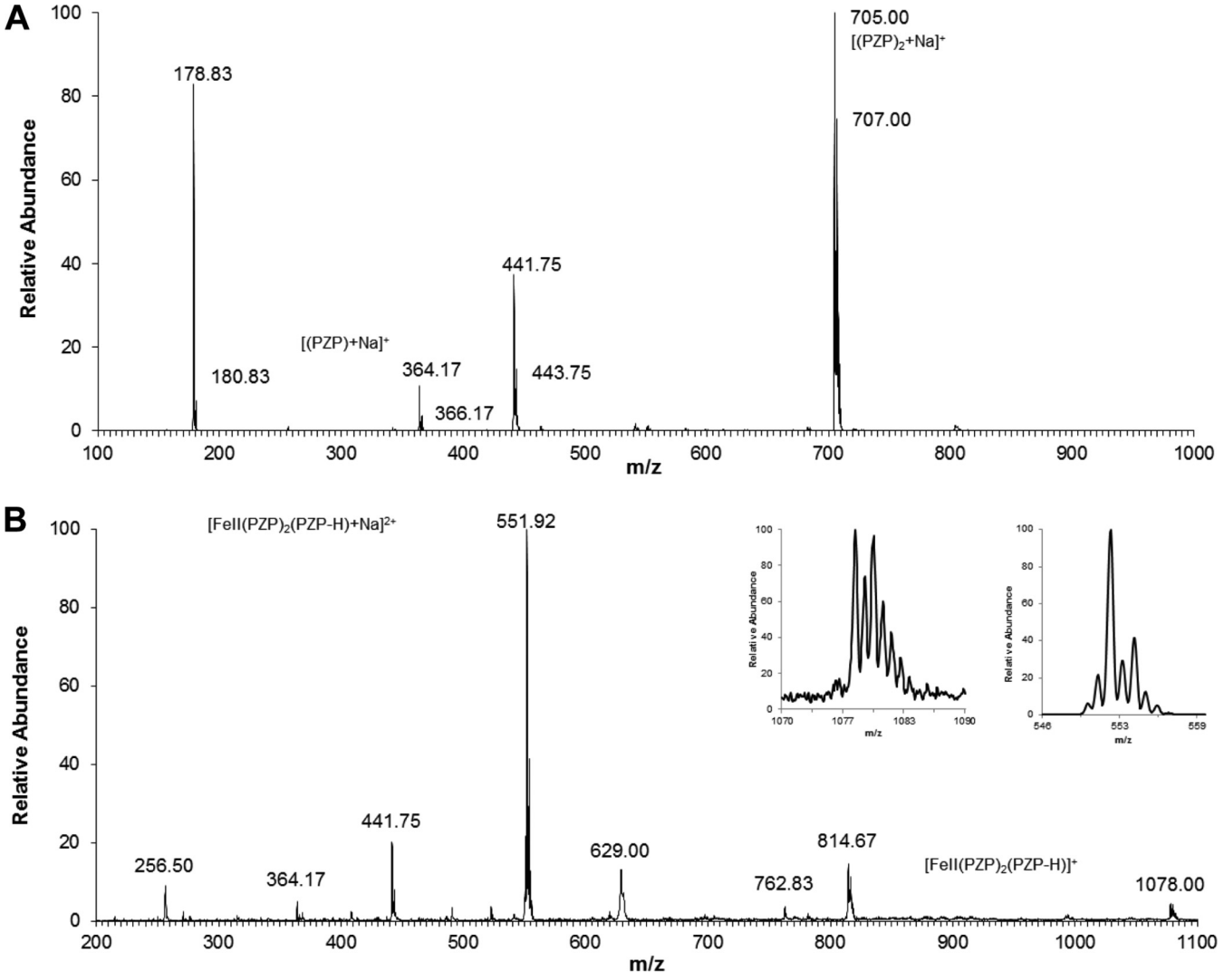

FIG 4 PZP chelates Fe^{2+}. (A) Electrospray mass spectra of 10 μM PZP. (B) Electrospray mass spectra of a solution of 10 μM PZP with 10 μM Fe^{2+}. The inset shows the isotopic pattern of the peaks at 551.92 and 1078.00 nm. All the reagents were dissolved in water-methanol (1:1, vol/vol).

$[PZP + Na]^+$), two Fe^{2+}-PZP complexes were detected at *m/z* 551.92 and *m/z* 1078.00 (Fig. 4B) when we mixed PZP and Fe^{2+}, with all displaying the typical iron isotopic pattern (Fig. 4B, insets). In both cases, species corresponding to the formation of the complex between PZP and Fe^{2+} showed a stoichiometry of 3:1 (*m/z* 551.92 $[Fe^{2+}(PZP)_2\ (PZP - H)Na]^{2+}$; *m/z* 1078.00 $[Fe^{2+}(PZP)_2\ (PZP - H)]^+$). All the other observed peaks did not fit with the classic iron isotopic pattern.

We further analyzed the ability of PZP to form complexes with iron by using UV-Vis spectroscopy. The compound was titrated with increasing amounts of Fe^{2+} (Fig. 5A). The intensities of the two bands at 275 and 310 nm, which were observed for PZP alone, decreased after addition of Fe^{2+}, whereas the absorbance in the region above 370 nm increased in intensity. Two isosbestic points were observed at 300 and 340 nm. These observations fit with the formation of a PZP-Fe^{2+} complex, since they can be explained by the delocalization of π electrons of the conjugated PZP ring system over the metal core upon PZP-iron binding. The titration curve confirmed the 3:1 stoichiometry (Fig. 5A, inset) determined in the ESI-MS spectrometry experiment. Figure 5B shows a possible chemical structure of the $[Fe(PZP)_3]^+$ complex. The conditional binding constant of the compound with Fe^{2+} was estimated at 400 nm by applying a method established for measuring the binding constants of complexes between flavonoids and iron (29). Since a strong binding constant was determined for the $[Fe(PZP)_3]^+$ complex (*K*, ~2×10^{11} mM), we performed competition experiments with ferrozine, a well-known Fe^{2+} chelator (*K*, 3.65×10^{15} mM) (38). Figure 5C shows the changes in absorbance of the Fe^{2+}-ferrozine complex after addition of PZP. The peak at 562 nm (Fe^{2+}-ferrozine) rose slightly in the first 30 min, possibly due to the formation of mixed ferrozine-Fe^{2+}-PZP complexes; similar complexes have been reported for amino acids and ferrozine (39). Absorbance increases in the region between 390 and 475 nm indicate the formation of the $[Fe(PZP)_3]^+$ complex. These findings indicate that the formation of this complex occurs while there is a dissociation of the ferrozine-Fe^{2+} complex. Altogether, these data confirm that PZP can strongly bind Fe^{2+} under physiological conditions.

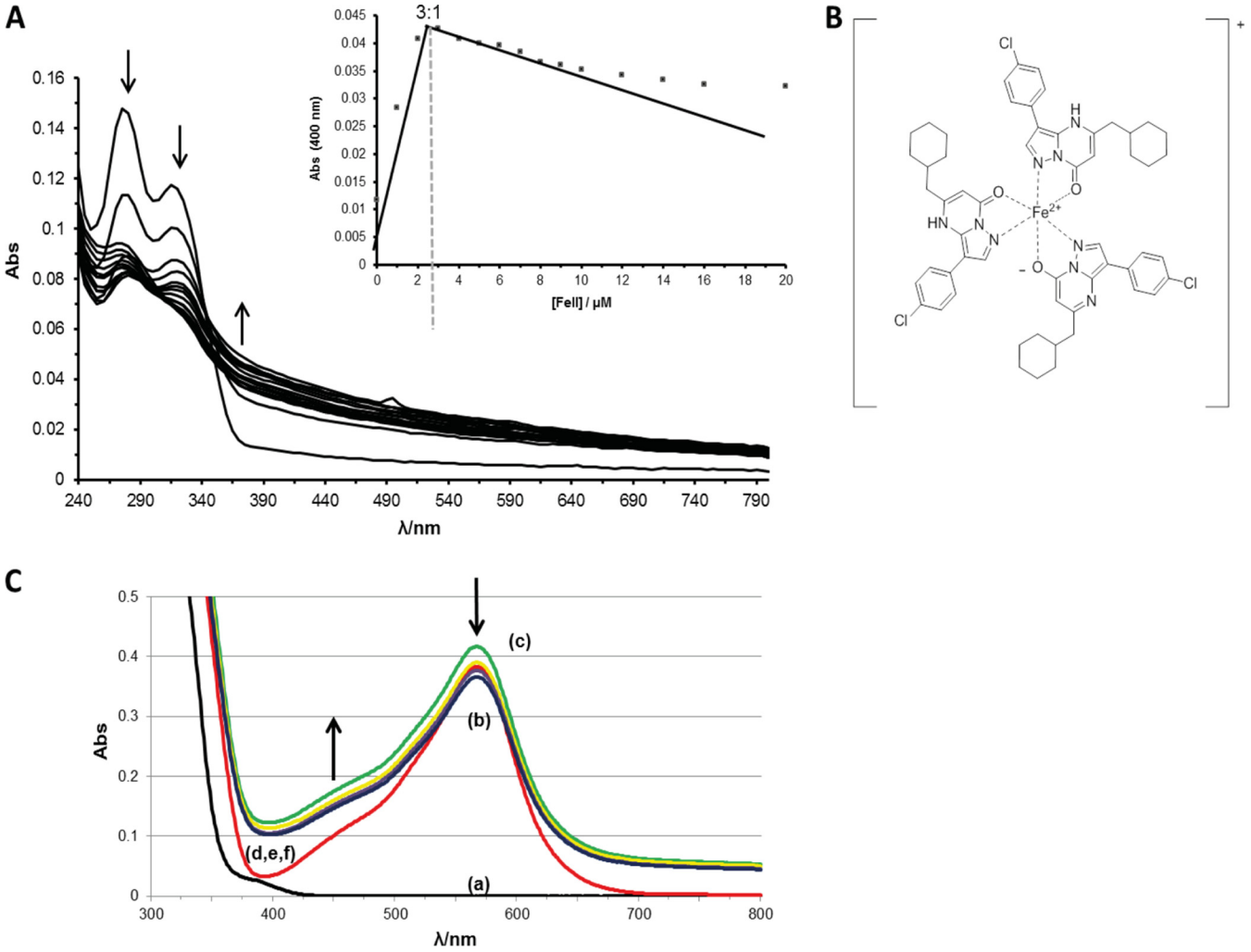

FIG 5 PZP competes with ferrozine by binding to iron in a 3:1 stoichiometric manner. (A) Spectroscopic titration of 10 μM PZP with Fe^{2+} (increments up to 10 μM were reached). (Inset) Absorbance of the PZP-Fe^{2+} complex at 400 nm as a function of Fe^{2+}. (B) Chemical structure of $(PZP)_3$-Fe^{2+} complex. (C) Competition experiment between ferrozine and PZP for Fe^{2+}. Curves: (a, black line), 60 μM ferrozine in 20 mM potassium phosphate buffer, pH 7.2 only; (b, red line) addition of 20 μM Fe^{2+}; (c, green line) addition of 60 μM PZP; (d to f, yellow, purple, and blue lines, respectively) addition of 60 μM PZP for 60 min (d), 90 min (e), or 120 min (f).

DISCUSSION

Nearly all mycobacteria produce the siderophores mycobactins (4, 5). The saprophytic nonpathogenic mycobacterium *M. smegmatis* produces the siderophore exochelin in addition to the mycobactins (6). Mycobactin-mediated iron uptake is dependent on the type VII mycobacterial secretion system ESX-3, while exochelin-mediated iron uptake is ESX-3 independent (18). The *M. tuberculosis esx-3* gene cluster is essential for *in vitro* growth (18, 20, 32–34), and *M. tuberculosis* is sensitive to PZP under standard iron conditions (15). In contrast, *M. smegmatis* ESX-3 is not essential for growth and *M. smegmatis* is protected against PZP in normal iron medium (18). Interestingly, although the species' requirement for ESX-3 coincides with their susceptibilities to PZP, we show that ESX-3 is in fact not the cellular target of this compound. Instead, we found that PZP apparently enters mycobacterial cells and chelates Fe^{2+} and starves the bacteria for intracellular iron.

In the environment, iron is available as Fe^{3+}. Thus, siderophores have been optimized to complex this ion. Once taken up by the cells though, Fe^{3+} is reduced to Fe^{2+}. The affinity of siderophores for Fe^{3+} is extraordinarily high, ranging from binding constant (K) of 10^{30} to 10^{52} M (40), far higher than PZP ($K \sim 2 \times 10^{11}$ mM). Thus, it is unlikely that this compound could effectively compete for extracellular iron. Instead, we postulate that the compound enters cells and chelates intracellular Fe^{2+}. The affinities of mycobacterial iron storage molecules like ferritin and bacterioferritin for Fe^{2+} are, to our knowledge, unknown. However, the Fe^{2+} affinity of the *Escherichia coli* bacterioferritin is estimated to be lower than K of $\sim 1.1 \times 10^7$ M, based on competition experiments with Zn^{2+} (41, 42). It is therefore likely that PZP binds Fe^{2+} intracellularly and deprives the cells of available iron storage and that the bacteria respond by upregulating the expression of iron acquisition systems. Given adequate access to extracellular iron, WT *M. smegmatis* can overcome the effects of starvation by increasing iron uptake. Similarly, mutations in *eccB3* increase intracellular iron levels further. The role of ESX-3 in mycobactin-mediated iron uptake is currently unknown. We speculate that ESX-3

secretes effector molecules important for utilization of mycobactin-bound iron. EccB3 could play a role in regulating secretion of such effectors, and mutations in the cytosolic tail of EccB3 might alter effector secretion. Regardless, depriving cells of iron results in inhibition of cell growth by PZP.

Wells et al. recently identified MmpS4/MmpL4 and MmpS5/MmpL5 as siderophore export systems in *M. tuberculosis* (13). An *M. tuberculosis* Δ*mmpS4* Δ*mmpS5* double mutant did not grow under iron-deplete conditions and was not fully rescued by adding hemoglobin as an iron source. However, the growth of *M. tuberculosis* Δ*mmpS4* Δ*mmpS5* with an additional mutation disrupting mycobactin synthesis was completely restored by hemoglobin, suggesting that the lack of mycobactin export leads to accumulation of the siderophore, potentially causing deleterious intracellular iron chelation (13). PZP could imaginably block exporters of mycobactins, perhaps by mimicking iron-chelating siderophores, and mutations in *eccB3* could make possible export of mycobactins through ESX-3. We have previously shown a small decrease in the pool of mycobactins and carboxymycobactins in the *M. smegmatis* Δ*esx-3* supernatant filtrate (18). However, this moderate change in exported mycobactins does not likely account for the severe Δ*esx-3*-mediated growth impairment seen with low iron (18), making a model based on blocking siderophore export via ESX-3 improbable as a mechanism of PZP.

A streptonigrin sensitivity assay recently suggested that intracellular iron decreases upon repression of *esx-3* expression (19). Conversely, Du Toit Loots et al. used metabolomic approaches to speculate that an *M. smegmatis esx-3* knockout mutant accumulates iron during iron-replete growth (43). It is likely that the resistant *eccB3* point mutations influence the iron uptake/assimilation-related properties of ESX-3, leading to increased influx of iron. However, this alone cannot explain the elevated iron accumulation by the *eccB3* mutant on low iron, as we did not see accumulation in the absence of PZP.

Although the *eccB3*(ΔN26) mutant accumulates iron also when grown under low-iron conditions, none of the three *M. smegmatis eccB3* mutants conferred resistance to PZP. However, we postulate that $eccB_3$ mutations enhance ESX-3-mediated iron uptake or assimilation, and it is likely that the subtle resistance effect (2.5-fold) seen in *M. tuberculosis* was not detectable in *M. smegmatis* simply because the cells were grown under iron-deficient conditions and lacked sufficient metal in the medium to rescue the cells from the compound.

A previous study on structure-activity relationships of compounds structurally related to PZP identified molecules with an inhibitory effect on *M. tuberculosis* 1-deoxy-D-xylulose 5-phosphate (DXS), an enzyme that combines the mechanisms of pyruvate decarboxylase and transketolase (44). Interestingly, DXS activity is absolutely dependent on divalent cations (45). It would be interesting to investigate PZP's activity on DXS as well as the chelating properties of these structurally related compounds.

The potential of iron chelators in TB therapeutics has been investigated previously. Chelators are able to restrict growth of *Mycobacterium avium* (46–48), while synthetic mycobactin analogues selectively inhibit *M. tuberculosis* growth (49). Additionally, iron chelation has proved to inhibit the cytotoxic effect of mycolactone, a macrolide toxin produced by *Mycobacterium ulcerans*, the causative agent of the necrotizing skin disease Buruli ulcer (50). A wide spectrum of chelators have furthermore been designed and synthesized in the search for the treatment of diseases ranging from acute myocardial infarction to neurodegenerative diseases and cancer (51–53). Together, these findings demonstrate a wide range of potential medical applications for iron chelators that is not restricted to antimycobacterial therapy.

ACKNOWLEDGMENTS

The work was supported by National Institutes of Health AI095208 and 1R21AI082484, R. J. Wolfe-Welch Foundation Chair in Science A-0015, the Research Council of Norway through its Centres of Excellence funding scheme, project number 223255/F50, and Research Council of Norway grant 220836/H10.

We gratefully acknowledge Kenan Murphy for providing pKM402 and for sharing protocols and guidance while constructing the *M. smegmatis eccB3* R14, N24H, and ΔN26 mutants by single-stranded recombineering. We also thank Claudio Villani for mass experiments.

REFERENCES

1. **Schaible UE, Kaufmann SHE.** 2004. Iron and microbial infection. Nat Rev Microbiol **2:**946–953. http://dx.doi.org/10.1038/nrmicro1046.
2. **Fontan P, Aris V, Ghanny S, Soteropoulos P, Smith I.** 2008. Global transcriptional profile of Mycobacterium tuberculosis during THP-1 human macrophage infection. Infect Immun **76:**717–725. http://dx.doi.org/10.1128/IAI.00974-07.
3. **Cellier MF, Courville P, Campion C.** 2007. Nramp1 phagocyte intracellular metal withdrawal defense. Microbes Infect **9:**1662–1670. http://dx.doi.org/10.1016/j.micinf.2007.09.006.
4. **Snow GA.** 1970. Mycobactins: iron-chelating growth factors from mycobacteria. Bacteriol Rev **34:**99–125.
5. **Lane SJ, Marshall PS, Upton RJ, Ratledge C, Ewing M.** 1995. Novel extracellular mycobactins: the carboxymycobactins from *Mycobacterium avium*. Tetrahedron Lett **36:**4129–4132. http://dx.doi.org/10.1016/0040-4039(95)00676-4.
6. **Macham LP, Ratledge C.** 1975. A new group of water-soluble iron-binding compounds from mycobacteria: the exochelins. J Gen Microbiol **89:**379–382. http://dx.doi.org/10.1099/00221287-89-2-379.
7. **Chan KG.** 2009. Exochelin production in Mycobacterium neoaurum. Int J Mol Sci **10:**345–353. http://dx.doi.org/10.3390/ijms10010345.
8. **Tullius MV, Harmston CA, Owens CP, Chim N, Morse RP, McMath LM, Iniguez A, Kimmey JM, Sawaya MR, Whitelegge JP, Horwitz MA, Goulding SJ.** 2011. Discovery and characterization of a unique mycobacterial heme acquisition system. Proc Natl Acad Sci U S A **108:**5051–5056. http://dx.doi.org/10.1073/pnas.1009516108.
9. **Jones CM, Niederweis M.** 2011. Mycobacterium tuberculosis can utilize heme as an iron source. J Bacteriol **193:**1767–1770. http://dx.doi.org/10.1128/JB.01312-10.
10. **Boradia VM, Malhotra H, Thakkar JS, Tillu VA, Vuppala B, Patil P, Sheokand N, Sharma P, Chauhan AS, Raje M, Raje CI.** 2014. Mycobacterium tuberculosis acquires iron by cell-surface sequestration and internalization of human holo-transferrin. Nat Commun **5:**4730. http://dx.doi.org/10.1038/ncomms5730.
11. **Jones CM, Niederweis M.** 2010. Role of porins in iron uptake by Mycobacterium smegmatis. J Bacteriol **192:**6411–6417. http://dx.doi.org/10.1128/JB.00986-10.
12. **Rodriguez GM, Smith I.** 2006. Identification of an ABC transporter required for iron acquisition and virulence in Mycobacterium tuberculosis. J Bacteriol **188:**424–430. http://dx.doi.org/10.1128/JB.188.2.424-430.2006.
13. **Wells RM, Jones CM, Xi Z, Speer A, Danilchanka O, Doornbos KS, Sun P, Wu F, Tian C, Niederweis M.** 2013. Discovery of a siderophore export system essential for virulence of Mycobacterium tuberculosis. PLoS Pathog **9:**e1003120. http://dx.doi.org/10.1371/journal.ppat.1003120.
14. **World Health Organization.** 2013. Tuberculosis. Fact sheet 104. World Health Organization, Geneva, Switzerland. http://www.who.int/mediacentre/factsheets/fs104/en/.content-type="access-date">Accessed 29 December 2014.
15. **Ioerger TR, O'Malley T, Liao R, Guinn KM, Hickey MJ, Mohaideen N, Murphy KC, Boshoff HIM, Mizrahi V, Rubin EJ, Sassetti CM, Barry CE, Sherman DR, Parish T, Sacchettini JC.** 2013. Identification of new drug targets and resistance mechanisms in Mycobacterium tuberculosis. PLoS One **8:**e75245. http://dx.doi.org/10.1371/journal.pone.0075245.

16. **Reddy PV, Puri RV, Chauhan P, Kar R, Rohilla A, Khera A, Tyagi AK.** 2013. Disruption of mycobactin biosynthesis leads to attenuation of Mycobacterium tuberculosis for growth and virulence. J Infect Dis **208:**1255–1265. http://dx.doi.org/10.1093/infdis/jit250.
17. **Bitter W, Houben ENG, Bottai D, Brodin P, Brown EJ, Cox JS, Derbyshire K, Fortune SM, Gao L-Y, Liu J, Gey Van Pittius NC, Pym AS, Rubin EJ, Sherman DR, Cole ST, Brosch R.** 2009. Systematic genetic nomenclature for type VII secretion systems. PLoS Pathog **5:**e1000507. http://dx.doi.org/10.1371/journal.ppat.1000507.
18. **Siegrist MS, Unnikrishnan M, McConnell MJ, Borowsky M, Cheng T-Y, Siddiqi N, Fortune SM, Moody DB, Rubin EJ.** 2009. Mycobacterial Esx-3 is required for mycobactin-mediated iron acquisition. Proc Natl Acad Sci U S A **106:**18792–18797. http://dx.doi.org/10.1073/pnas.0900589106.
19. **Serafini A, Pisu D, Palù G, Rodriguez GM, Manganelli R.** 2013. The ESX-3 secretion system is necessary for iron and zinc homeostasis in Mycobacterium tuberculosis. PLoS One **8:**e78351. http://dx.doi.org/10.1371/journal.pone.0078351.
20. **Serafini A, Boldrin F, Palu G, Manganelli R.** 2009. Characterization of a Mycobacterium tuberculosis ESX-3 conditional mutant: essentiality and rescue by iron and zinc. J Bacteriol **191:**6340–6344. http://dx.doi.org/10.1128/JB.00756-09.
21. **Siegrist MS, Steigedal M, Ahmad R, Mehra A, Dragset MS, Schuster BM, Philips JA, Carr SA, Rubin EJ.** 2014. Mycobacterial esx-3 requires multiple components for iron acquisition. mBio **5**(3)**:**e01073-14. http://dx.doi.org/10.1128/mBio.01073-14.
22. **Snapper SB, Melton RE, Mustafa S, Kieser T, Jacobs WR.** 1990. Isolation and characterization of efficient plasmid transformation mutants of Mycobacterium smegmatis. Mol Microbiol **4:**1911–1919. http://dx.doi.org/10.1111/j.1365-2958.1990.tb02040.x.
23. **van Kessel JC, Hatfull GF.** 2007. Recombineering in Mycobacterium tuberculosis. Nat Methods **4:**147–152. http://dx.doi.org/10.1038/nmeth996.
24. **Ehrt S.** 2005. Controlling gene expression in mycobacteria with anhydrotetracycline and Tet repressor. Nucleic Acids Res **33:**e21. http://dx.doi.org/10.1093/nar/gni013.
25. **van Kessel JC, Hatfull GF.** 2008. Efficient point mutagenesis in mycobacteria using single-stranded DNA recombineering: characterization of antimycobacterial drug targets. Mol Microbiol **67:**1094–1107. http://dx.doi.org/10.1111/j.1365-2958.2008.06109.x.
26. **Cha RS, Zarbl H, Keohavong P, Thilly WG.** 1992. Mismatch amplification mutation assay (MAMA): application to the c-H-ras gene. Genome Res **2:**14–20. http://dx.doi.org/10.1101/gr.2.1.14.
27. **Palomino JC, Martin A, Camacho M, Guerra H, Swings J, Portaels F.** 2002. Resazurin microtiter assay plate: simple and inexpensive method for detection of drug resistance in Mycobacterium tuberculosis. Antimicrob Agents Chemother **46:**2720–2722. http://dx.doi.org/10.1128/AAC.46.8.2720-2722.2002.
28. **Bradford MM.** 1976. A rapid and sensitive method for the quantitation of microgram quantities of protein utilizing the principle of protein-dye binding. Anal Biochem **72:**248–254. http://dx.doi.org/10.1016/0003-2697(76)90527-3.
29. **Perez CA, Wei Y, Guo M.** 2009. Iron-binding and anti-Fenton properties of baicalein and baicalin. J Inorg Biochem **103:**326–332. http://dx.doi.org/10.1016/j.jinorgbio.2008.11.003.
30. **Sonnhammer EL, von Heijne G, Krogh A.** 1998. A hidden Markov model for predicting transmembrane helices in protein sequences. Proc Int Conf Intell Syst Mol Biol **6:**175–182.
31. **Krogh A, Larsson B, von Heijne G, Sonnhammer EL.** 2001. Predicting transmembrane protein topology with a hidden Markov model: application to complete genomes. J Mol Biol **305:**567–580. http://dx.doi.org/10.1006/jmbi.2000.4315.
32. **Zhang YJ, Ioerger TR, Huttenhower C, Long JE, Sassetti CM, Sacchettini JC, Rubin EJ.** 2012. Global assessment of genomic regions required for growth in Mycobacterium tuberculosis. PLoS Pathog **8:**e1002946. http://dx.doi.org/10.1371/journal.ppat.1002946.
33. **Sassetti CM, Boyd DH, Rubin EJ.** 2003. Genes required for mycobacterial growth defined by high density mutagenesis. Mol Microbiol **48:**77–84. http://dx.doi.org/10.1046/j.1365-2958.2003.03425.x.
34. **Griffin JE, Gawronski JD, DeJesus MA, Ioerger TR, Akerley BJ, Sassetti CM.** 2011. High-resolution phenotypic profiling defines genes essential for mycobacterial growth and cholesterol catabolism. PLoS Pathog **7:**e1002251. http://dx.doi.org/10.1371/journal.ppat.1002251.
35. **Rodriguez GM, Voskuil MI, Gold B, Schoolnik GK, Smith I.** 2002. ideR, an essential gene in Mycobacterium tuberculosis: role of IdeR in iron-dependent gene expression, iron metabolism, and oxidative stress response. Infect Immun **70:**3371–3381. http://dx.doi.org/10.1128/IAI.70.7.3371-3381.2002.
36. **Krithika R, Marathe U, Saxena P, Ansari MZ, Mohanty D, Gokhale RS.** 2006. A genetic locus required for iron acquisition in Mycobacterium tuberculosis. Proc Natl Acad Sci U S A **103:**2069–2074. http://dx.doi.org/10.1073/pnas.0507924103.
37. **Ryndak MB, Wang S, Smith I, Rodriguez GM.** 2010. The Mycobacterium tuberculosis high-affinity iron importer, IrtA, contains an FAD-binding domain. J Bacteriol **192:**861–869. http://dx.doi.org/10.1128/JB.00223-09.
38. **Gibbs CR.** 1976. Characterization and application of ferrozine iron reagent as a ferrous iron indicator. Anal Chem **48:**1197–1201. http://dx.doi.org/10.1021/ac50002a034.
39. **Berlett BS, Levine RL, Chock PB, Chevion M, Stadtman ER.** 2001. Antioxidant activity of ferrozine-iron-amino acid complexes. Proc Natl Acad Sci U S A **98:**451–456. http://dx.doi.org/10.1073/pnas.98.2.451.
40. **Zheng T, Nolan EM.** 2012. Siderophore-based detection of Fe(III) and microbial pathogens. Metallomics **4:**866–880. http://dx.doi.org/10.1039/c2mt20082a.
41. **Le Brun NE, Keech AM, Mauk MR, Mauk AG, Andrews SC, Thomson AJ, Moore GR.** 1996. Charge compensated binding of divalent metals to bacterioferritin: H^+ release associated with cobalt(II) and zinc(II) binding at dinuclear metal sites. FEBS Lett **397:**159–163. http://dx.doi.org/10.1016/S0014-5793(96)01172-6.
42. **Le Brun NE, Andrews SC, Guest JR, Harrison PM, Moore GR, Thomson AJ.** 1995. Identification of the ferroxidase centre of Escherichia coli bacterioferritin. Biochem J **312:**385–392.
43. **Loots DT, Meissner-Roloff RJ, Newton-Foot M, van Pittius NCG.** 2012. A metabolomics approach exploring the function of the ESX-3 type VII secretion system of M. smegmatis. Metabolomics http://dx.doi.org/10.1007/s11306-012-0481-x.
44. **Mao J, Eoh H, He R, Wang Y, Wan B, Franzblau SG, Crick DC, Kozikowski AP.** 2008. Structure-activity relationships of compounds targeting mycobacterium tuberculosis 1-deoxy-d-xylulose 5-phosphate synthase. Bioorg Med Chem Lett **18:**5320–5323. http://dx.doi.org/10.1016/j.bmcl.2008.08.034.
45. **Bailey AM, Mahapatra S, Brennan PJ, Crick DC.** 2002. Identification, cloning, purification, and enzymatic characterization of Mycobacterium tuberculosis 1-deoxy-D-xylulose 5-phosphate synthase. Glycobiology **12:**813–820. http://dx.doi.org/10.1093/glycob/cwf100.
46. **Nunes A, Podinovskaia M, Leite A, Gameiro P, Zhou T, Ma Y, Kong X, Schaible UE, Hider RC, Rangel M.** 2010. Fluorescent 3-hydroxy-4-pyridinone hexadentate iron chelators: intracellular distribution and the relevance to antimycobacterial properties. J Biol Inorg Chem **15:**861–877. http://dx.doi.org/10.1007/s00775-010-0650-1.
47. **Moniz T, Nunes A, Silva AMG, Queirós C, Ivanova G, Gomes MS, Rangel M.** 2013. Rhodamine labeling of 3-hydroxy-4-pyridinone iron chelators is an important contribution to target Mycobacterium avium infection. J Inorg Biochem **121:**156–166. http://dx.doi.org/10.1016/j.jinorgbio.2013.01.002.
48. **Fernandes SS, Nunes A, Gomes AR, de Castro B, Hider RC, Rangel M, Appelberg R, Gomes MS.** 2010. Identification of a new hexadentate iron chelator capable of restricting the intramacrophagic growth of Mycobacterium avium. Microbes Infect **12:**287–294. http://dx.doi.org/10.1016/j.micinf.2010.01.003.
49. **Juárez-Hernández RE, Franzblau SG, Miller MJ.** 2012. Syntheses of mycobactin analogs as potent and selective inhibitors of Mycobacterium tuberculosis. Org Biomol Chem **10:**7584. http://dx.doi.org/10.1039/c2ob26077h.
50. **Gronberg A, Zettergren L, Bergh K, Stahle M, Heilborn J, Angeby K, Small PL, Akuffo H, Britton S.** 2010. Antioxidants protect keratinocytes against M. ulcerans mycolactone cytotoxicity. PLoS One **5:**e13839. http://dx.doi.org/10.1371/journal.pone.0013839.
51. **Li X, Jankovic J, Le W.** 2011. Iron chelation and neuroprotection in neurodegenerative diseases. J Neural Transm **118:**473–477. http://dx.doi.org/10.1007/s00702-010-0518-0.
52. **Kalinowski DS, Richardson DR.** 2005. The evolution of iron chelators for the treatment of iron overload disease and cancer. Pharmacol Rev **57:**547–583. http://dx.doi.org/10.1124/pr.57.4.2.
53. **Hider RC, Roy S, Ma YM, Le Kong X, Preston J.** 2011. The potential application of iron chelators for the treatment of neurodegenerative diseases. Metallomics **3:**239–249. http://dx.doi.org/10.1039/c0mt00087f.